Modelling of Agitation Rate Effect on Temperature Homogenization, Mechanical Strength, and Residual Stresses in Quenched SAE 1025 Steel

T. S. Olabamiji[1]* and S. M. Adedayo[2]

[1] *Department of Mechanical Engineering, Redeemer's University, Ede, Osun State, Nigeria*
[2] *Department of Mechanical Engineering, University of Ilorin, Ilorin, Kwara State, Nigeria*
*Corresponding author: bamijit@run.edu.ng

Received 05/08/2025; accepted 10/01/2026
https://doi.org/10.4152/pea.2027450519

Abstract

Residual stresses formed during quenching can significantly impact the integrity of engineering components. This study examined how varying immersion speeds in water affected both mechanical behavior and residual stress distribution in SAE 1025 steel. To achieve this, a hybrid approach combining finite element simulations (using ANSYS 2020 R1 and JMatPro) with controlled laboratory experiments was employed. The immersion speed control mechanism was developed and calibrated. Steel samples were quenched at five immersion speeds, ranging from 0.05 to 0.8 m/s. Metallographic analysis, Vickers microhardness testing and tensile testing were assessed and then compared to simulation predictions. A significant finding was the 83% reduction in maximum residual stress as immersion speed increased from 0.2 to 0.8 m/s. Furthermore, residual stress was significantly lower at the leading (first-contact) end of each sample and higher at the trailing end. Simulation results showed strong agreement with experimental findings, achieving an average error of 7.5% across the temperature range and a correlation coefficient (R^2) of 0.97. Ultimately, the prediction of residual stress distributions achieved in this study will enable the production of safer and more durable components, critical for demanding engineering applications where performance and integrity are non-negotiable.

Keywords: cooling rate; deformation; heat treatment; homogenization; immersion speed; residual stress.

Introduction•

Quenching is a critical process aimed at enhancing the mechanical strength and performance of steels by rapid cooling from austenitizing temperatures. Final properties produced depend upon the carbon content of the material, the temperature

•The abbreviation and symbols definition list is in pages 650-51.

to which it was heated, holding time and cooling rate [1-5]. The ultimate objectives of the heat treater during the quenching process are to control percentage of preferred phase (martensite), shape of its microstructure, residual stresses and component deformation (dimension instability) [6, 7]. Proper quenching techniques and parameters are critical to achieving the desired combination.

SAE 1025 steel is a medium-low carbon steel containing approximately 0.737% manganese and 0.013% chromium. It is widely used in engineering applications because of its good balance of strength, ductility, weldability and machinability. The steel is readily available, cost-effective and easy to process, making it a common choice in manufacturing and structural applications. Its relatively low carbon content gives it good formability and weldability, but limits its as-received strength. For this reason, heat treatment, particularly quenching, is often applied to improve the steel's mechanical performance. The presence of manganese also enhances hardenability and increases carbon equivalent, making the steel responsive to heat treatment without compromising its weldability. These combined properties make SAE 1025 an ideal material for studying the effects of quenching parameters, such as immersion speed, on mechanical properties [8-11].

Hardenability is indicated by the critical cooling rate depicted on Time-Temperature Transformation curve of a steel of known composition. To achieve the desired hardening, quenching intensity can be varied by the type of quenchant, its concentration, temperature, and the state of agitation [12-15]. Immersion quenching duration, stirring speed or injection pressure are forms of agitation of cooling media to improve quenching conditions at high cooling rates [16]. Consequently, development of residual stress is one of the inevitable outcomes of high cooling rate during quenching, the magnitude of which depends on cooling histories at different parts of the specimen. Residual stress develops as a result of a mismatch in the deformation of material caused by several reasons, including temperature gradient [17]. Because of these gradients, plastic inhomogeneous flow occurs, resulting in residual stresses and dimensional instability.

Integrity and service performance of structural components can be critically compromised by the presence of residual stresses, particularly tensile residual stresses, which may promote crack initiation and propagation under service loading conditions[18]. Cracks can be generated when internal stresses exceed the strength of the quenched component. A catastrophic failure may occur instantly if these stresses are acting corresponding to the direction of the applied load [19]. An investigation was conducted to evaluate the reliability of a mathematical model that is incorporated into DEFORM-3D software. The impact of immersion speed on strength, residual stresses and distortions that resulted from the heat treatment used to harden SAE 5160 steel bar was assessed. Various rates of immersion (0.05-0.14 m/s) were examined. Deformation and residual stress may be reduced within predetermined ranges of

immersion speeds, based on the results [18]. The impact of quenchant circulation, agitation and specimen orientation on heat transfer coefficient during quenching was investigated, and how this in turn affected residual stress formation in the quenched product [20].

Regardless of immersion rate, achieving uniform cooling across the material's surface is crucial for consistent and predictable results. Uneven cooling can lead to distortions, warping or variations in material properties, compromising the final quality of the product after quenching.

Residual stresses that develop during quenching, mainly due to non-uniform cooling, strongly influence safety, durability and overall performance of engineering components. Although quenching has been widely studied, the role of immersion speed, a controllable parameter with significant potential impact, is still not well understood. Most existing studies concentrates on factors such as cooling media, agitation and bath temperature, but offer limited explanation of how controlled immersion speeds influence heat extraction (particularly during film boiling stage), microstructural evolution, cooling homogeneity and resulting residual stress distribution in steels like SAE 1025. Herein, the focus was to numerically investigate how changes in immersion speed affect cooling rate, deformation, residual stresses and mechanical strength of SAE 1025 steel.

Materials and methods

Table 1 shows chemical composition of SAE 1025 steel used in this study.

Table 1: Chemical composition of SAE 1025 steel.

Element	**Percentage** (wt%)
Mn	0.737
Cr	0.13
Si	0.22
P	0.045
S	0.047
C	0.25
Ni	0.092
Cu	0.27
Nb	0.0001
Al	0.02
B	0.0001
W	0.0001
Mo	0.0001
V	0.0001
Ti	0.007
Fe	97.178

Thermo-physical properties of SAE 1025 Steel

Development of JMatPro (Material simulation software) has significantly addressed the challenge of insufficient material data for computer-aided engineering simulation. Thermo-physical properties of SAE 1025 simulated by JMaPro are given in Fig. 1.

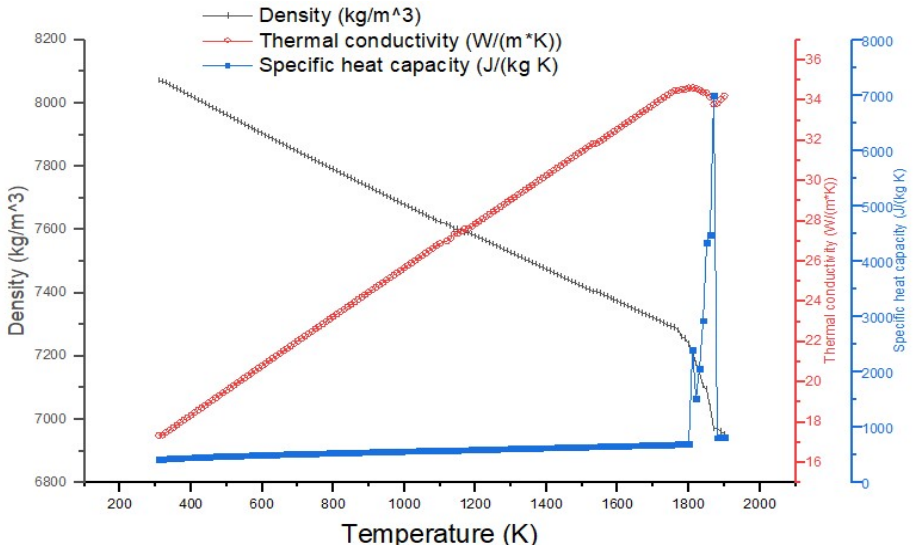

Figure 1: Temperature-dependent thermo-physical parameters of SAE 1025 steel (density, thermal conductivity and specific heat).

Quenching modeling

In this study, ANSYS Fluent 2020R1 and JMaPro were used for nonlinear thermal and mechanical analysis. A materials' property database was created to input data for simulating heat treatment processes. Physical and thermal properties of the unquenched component were generated with JMaPro and derived based on measured elemental composition of SAE 1025 steel. Simulation required 3900 secs of computation time on a personal computer equipped with 8 GB RAM and an Intel Core i5-2520M CPU running at 2.50 GHz.

Thermal analysis

The study employed a time step of 0.1 secs for unsteady simulations, with the quenchant's initial temperature at 300 K [21]. The simulation was performed on a specimen with a diameter of 5 mm and a height of 30 mm, using a 3D approach with a symmetric axis. Overall number of elements in rod and bath was 52,800 and 54,431, respectively, while total number of nodes was 55,752 and 9,986. Fig. 2 shows typical configuration of the meshed rod. To reduce effects of excessive temperature rise, a liquid pool measuring 2200 mm in height and 100 mm in radius was used to help dissipate heat more effectively. The model was incorporated into CFD code Ansys Fluent 2020R1, specifically within the mixture model. Thermophysical properties of SAE 1025 steel, tailored to its specific alloy composition, were sourced from JMatPro database to ensure accuracy and relevance to the material under study [22-24]. For each node, initial temperature was set to 1100 K, as predicted by JMatPro, with grain size (ASTM 9). Historical residual stresses were taken to be negligible [22]. The modeling process encompasses all transitions from austenite to martensite.

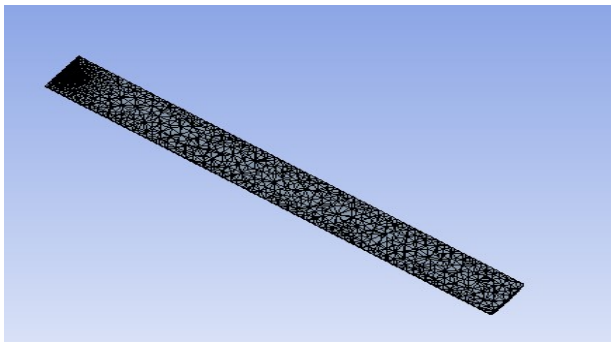

Figure 2: Typical configuration of the sectioned meshed rod.

Steel properties are dependent on both present phase and temperature, establishing a comprehensive framework for capturing thermal and mechanical behavior throughout phase transformation process. Martensite transition temperature for steel calculated by JMatPro was 688 K.

Governing equations

Continuity equation

Continuity equation is as given [25]:

$$\frac{\partial}{\partial t}(\rho_m) + \nabla.(\rho_m \vec{v}) = 0 \tag{1}$$

$$\vec{v}_m = \frac{\sum_{k=1}^{n} \alpha_k \rho_k \vec{v}_k}{\rho_m} \tag{2}$$

Momentum equation

Momentum equation for the quenchant can be derived by summing individual momentum equations for all phases. It can be expressed as [25]:

$$\frac{\partial}{\partial t}(\rho_m \vec{v}_m) + \nabla.(\rho_m \vec{v}_m \vec{v}_m) = -\nabla p + \nabla.\left[\mu_m\left(\nabla \vec{v}_m + \nabla \vec{v}_m^{T}\right)\right] + \rho_m \vec{g} \vec{F} + \nabla.\left(\sum_{k=1}^{n} \alpha_k \rho_k \vec{v}_{dr,k} \vec{v}_{dr,k}\right) \tag{3}$$

$$\mu_m = \sum_{k=1}^{n} \alpha_k \mu_k \tag{4}$$

$$\vec{v}_{dr,k} = \vec{v}_k - \vec{v}_m \tag{5}$$

Energy equation

Energy equation takes the following form:

$$\frac{\partial}{\partial t}\sum_{k=1}^{n}(\alpha_k \rho_k E_k) + \nabla.\sum_{k=1}^{n}\left(\alpha_k \vec{v}_k (\rho_k E_k + p)\right) = \nabla.\left(k_{eff} \nabla T\right) + S_E \tag{6}$$

Modeling of the temperature fields in the rod

The mathematical model for heat conduction problem is discussed in Cartesian coordinates as [25]:

$$\frac{\partial}{\partial x}(k\frac{\partial T}{\partial x})+\frac{\partial}{\partial y}(k\frac{\partial T}{\partial y})+\frac{\partial}{\partial z}(k\frac{\partial T}{\partial z})+Q=\rho c_p\frac{\partial T}{\partial t} \quad (7)$$

Experimental work

Design of immersion speed control mechanism

An electrically controlled system that ensures precise and repeatable immersion speeds for improved quenching outcomes was designed and constructed. Speed calibration was done by using a tachometer and a potentiometer. Fig. 3 shows the experimental setup for quenching under varying immersion speeds.

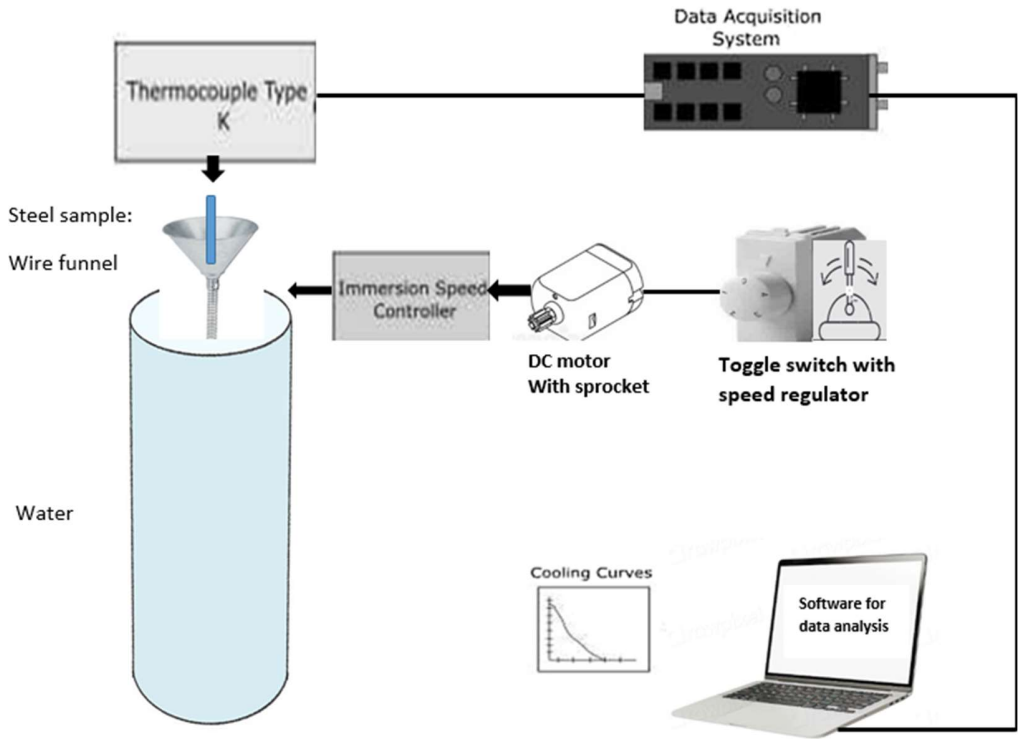

Figure 3: Flow chart for obtaining cooling profiles for steel samples with different immersion speeds using a temperature data logger.

Tensile test

Three specimens were prepared for each of the four immersion speeds considered. Tensile tests were conducted on as-received and quenched SAE 1025 steel samples. The obtained steel was machined on a precision lathe machine in Engineering Workshop at Redeemers' University Ede, following the standard shown in Fig. 4. Dimensions follows specification used in the simulation for validation.

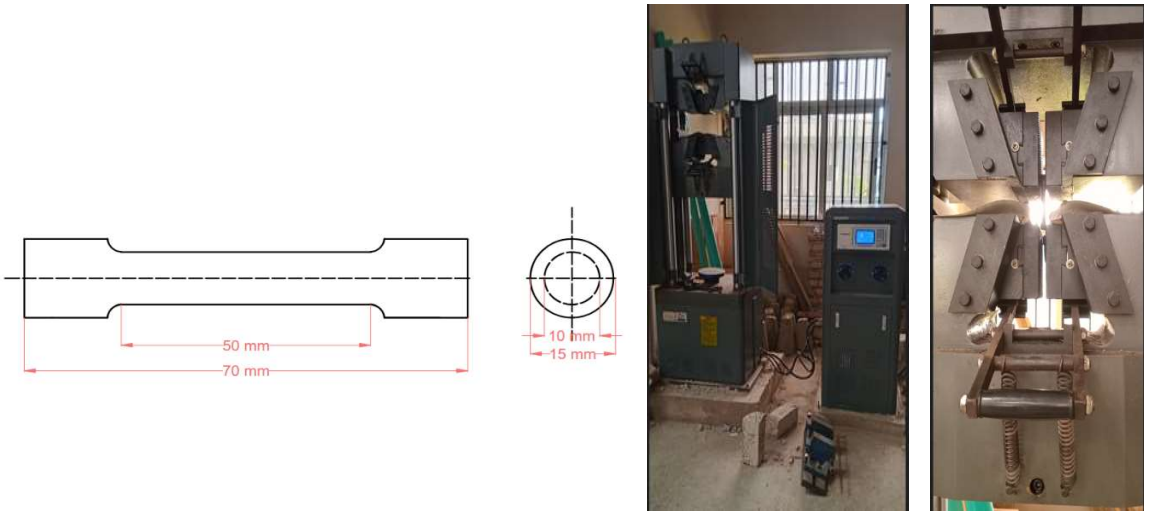

(a) **(b)**

Figure 4: Tensile test- **(a)** specimen geometry and **(b)** universal testing machine.

In preparing the sample for tensile testing, care was taken to ensure accuracy and consistency. Steel rods were first cut into standardized dimensions based on ASTM E8M requirements. Surface imperfections were removed using fine-grade emery paper to avoid stress concentration during the test. The tensile test was conducted in the structural laboratory using a universal testing machine (OKH–1000–WE, Serial No. 2112E19). Key data, such as yield strength, ultimate tensile strength and yield strength, were captured automatically by the machine's digital interface.

Heating and quenching procedure

The second phase of the experiment was conducted in Metallurgical Laboratory at the Redeemers' University, Ede, Nigeria. This involved heating the specimens to the austenitizing temperature of 847 ºC. Transient temperature readings were captured using a 4-channel temperature meter/data logger (Model No TM-947SD) instrumented with a K-type thermocouple. The specimens were maintained at this temperature for 24 min, and then quenched at varying immersion speeds (0.2, 0.4, 0.6 and 0.8 m/s), using water as quenchant.

Microstructural test

Microstructural study was achieved using Scanning electron microscope **(**SEM, Hitachi SU 3500 scanning microscope, Tokyo), at Afe Babalola University, Oye, in addition to the metallurgical microscope (Model: 4XC-W, multiple: 100 - 1000X) at Redeemers University. An image analysis software (ImageJ) was used to evaluate percentage phase composition of martensite in SEM micrographs of the quenched steel sample. This phase focused on examining how quenching at varying speeds influenced phase distribution in the steel.

Hardness test

Before testing, the specimens were carefully mounted in phenolic powder, then ground and polished to achieve a smooth and reflective surface suitable for accurate examination. A direct load of 1 Kg was applied for a dwell time of 15 secs, and hardness readings were recoded following ASTM E384. Three specimens for each immersion speed were tested. Three indentations were made on each sample. An average was calculated from the values obtained to provide a representative measure for analysis. Hardness was assessed using a Vickers Micro-hardness tester (Model: HV-1000, Serial No H115152) in the metallurgical laboratory at Redeemer's University, Ede, Nigeria.

Results and discussion

Simulation results for cooling rate, residual stresses, deformation and mechanical strength of quenched SAE 1025 steel rod are hereby presented. A complex combination of thermal, mechanical and phase transformations was executed.

Geometry and mesh independence

An appropriate number of grids was obtained by carrying out grid independence with immersion speeds of 0.8 m/s, as presented in Fig. 5. A Grid size of 0.3 mm was adopted in the simulation based on computational time and accuracy required.

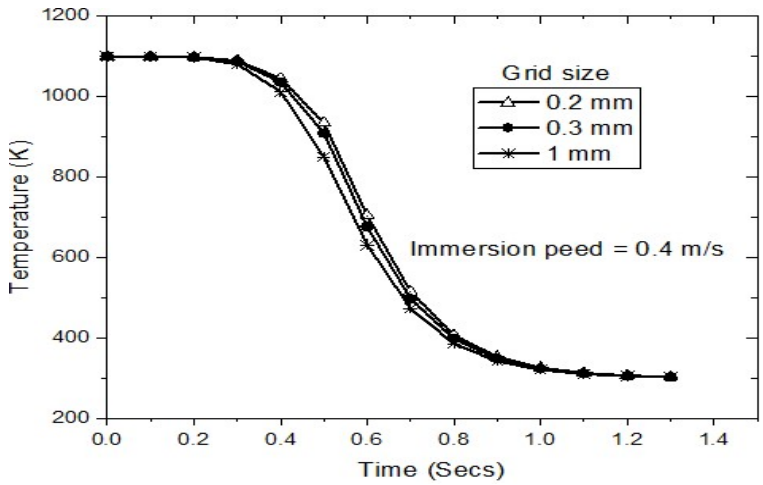

Figure 5: Grid independence test results at location (0.5 h) at 0.8 immersion speeds.

Thermal analysis

Effect of immersion speed on cooling rate in quenched SAE 1025 steel

Fig. 6 shows a section of the geometry used in the simulation, indicating point (0.5 h). Cooling curves at different immersion speeds are shown in Fig. 7. Maximum cooling rates increase with immersion speed, as reported by previous researchers [18].

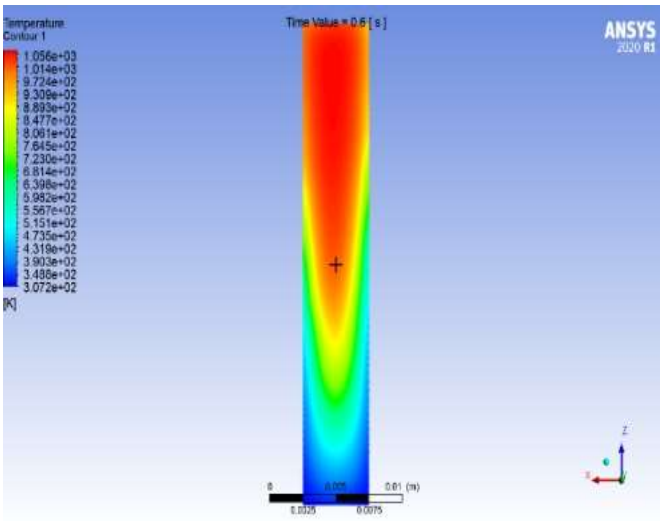

Figure 6: Section of the geometry showing location (0.5 h).

This was attributable to rapid heat removal from the work piece, as a result of the rapid motion of the specimen through the quenchant, which enhances heat transfer across workpiece boundaries. Less time is available for development of high thermal gradients, which result in residual stresses in the specimen.

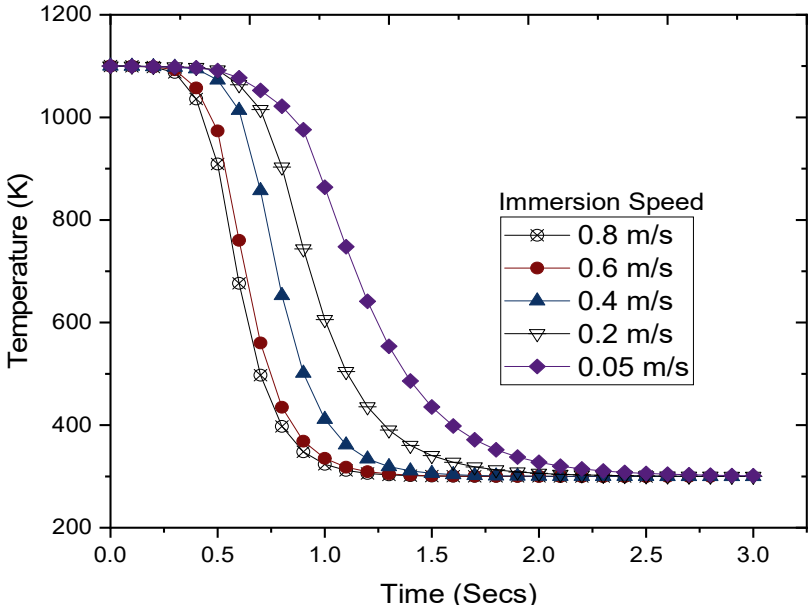

Figure 7: Cooling curve of location (0.5 h) at different immersion speeds in water.

Cooling profile at different locations along the central axis of the specimen

Fig. 8 shows locations (A = 0.1 h, B = 0.5 h and C = 0.7 h) along the central axis on the specimen quenched with 0.4 m/s immersion speed.

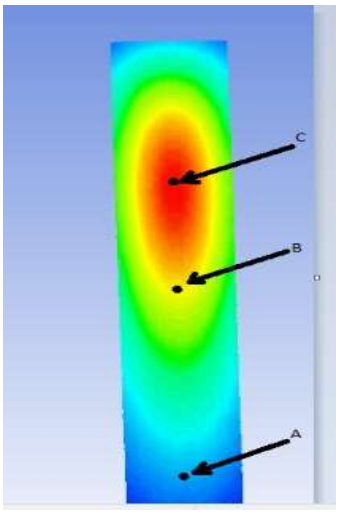

Figure 8: Section of geometry indicating points A, B, and C.

Fig. 9 shows cooling history at each point. Temperature at each location decreased exponentially as a function of time, as it cooled from 1100 to 300 K.

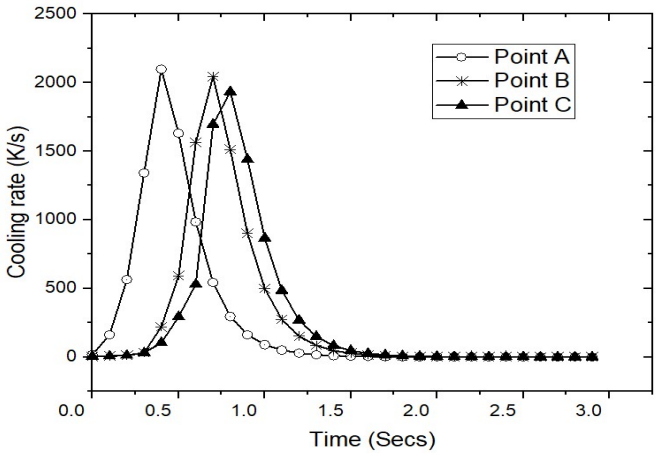

Figure 9: Cooling rate variation at selected points along central axis at 0.4 m/s immersion speed.

Point A has the highest cooling rate, due to its location at the leading end of the specimen. The leading end makes contact with the quenchant first. Heat is rapidly conducted away from the surface, causing it to cool faster. The trailing end of the steel maintains a higher temperature than the leading end at the commencement of immersion, but as the specimen moves through the quenchant, it loses heat to the surrounding liquid. This results in a time lag in the cooling kinetics at different locations in the specimen, which could contribute significantly to a differential deformation rate and eventual residual stresses.

Effect of immersion speed on maximum deformation of the quenched steel sample

Fig. 10 shows maximum deformation (dimension instability) produced in the specimen after quenching with different immersion speeds. Maximum deformations of 0.1, 0.056, 0.022, 0.018 and 0.013 mm were obtained with immersion speeds of 0.05, 0.2, 0.4, 0.6, and 0.8 m/s, respectively. An increase in immersion speed results in lower deformation caused by a reduction in thermal gradient and an increase in cooling rate caused by faster homogenization of the medium.

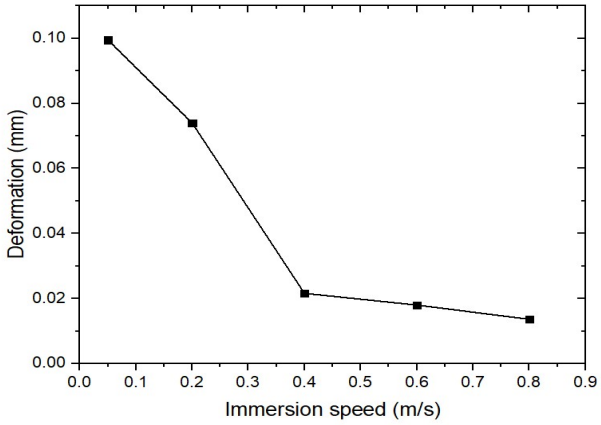

Figure 10: Maximum deformation at different immersion speeds.

Analysis of residual stresses in quenched SAE 1025 steel

Effect of immersion rate on longitudinal stress profiles in quenched SAE 1025 steel

Fig. 11 shows residual stress map generated for 0.4 m/s immersion speed.

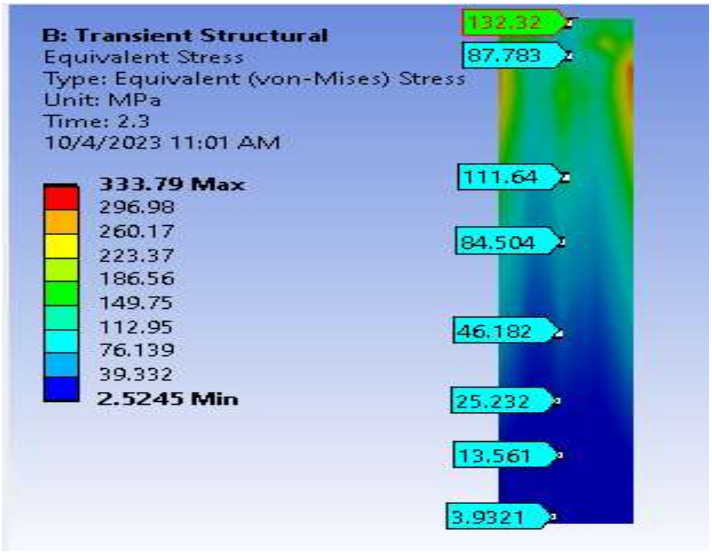

Figure 11: Longitudinal residual stress map at 0.4 m/s immersion speed.

Fig. 12 shows residual stresses produced along longitudinal axis of the specimen at different immersion speeds. It can be observed that lower residual stress values were obtained at leading end, and higher values at trailing end of quenched sample, which follows findings of [24]. Residual stress values of 10 and 223 MPa, with an immersion speed of 0.2 m/s, were obtained at leading and trailing ends, respectively. Lower cooling rate at trailing edge allows grains and transformation products to grow larger, because diffusion-controlled transformations have more time to occur. These coarse grains do not accommodate plastic deformation effectively, and, when combined with thermal and transformation mismatches that develop during cooling, result in higher residual stress in trailing-edge region [26].

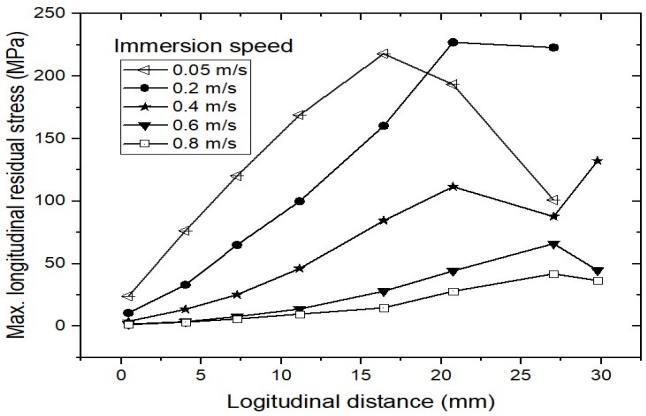

Figure 12: Longitudinal direction residual stress distribution at different immersion speeds.

Variation in residual stress across sample radius due to immersion speed

Fig. 13 shows residual stress map generated along the radius of the steel bar at 0.4 m/s immersion speed.

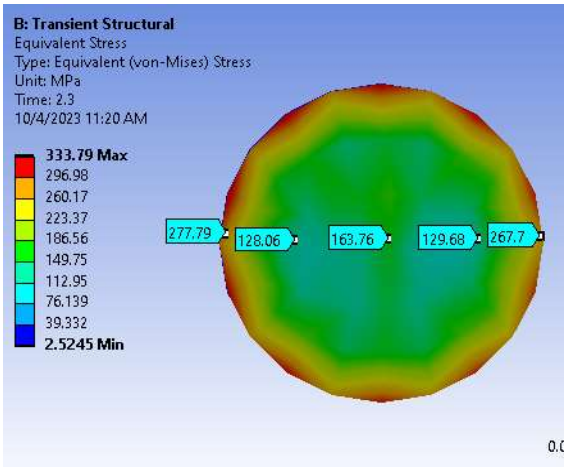

Figure 13: Residual stress map along radial direction for 0.4 m/s immersion speed.

Fig. 14 shows residual stress produced along the radius of the specimen at different immersion speeds. Higher residual stress values were obtained at the outer region, and lower values at the core of the specimen, following findings of [27-29]. A steep thermal gradient makes the surface cool much faster, so it transforms to martensite earlier and undergoes its characteristic volume expansion. Meanwhile, the core remains hotter for longer and resists both the surface's thermal contraction and its transformational strain. This imbalance between how the surface and core cool and transform creates a strong transformational gradient, which in turn leads to high residual stresses developing in the surface region.

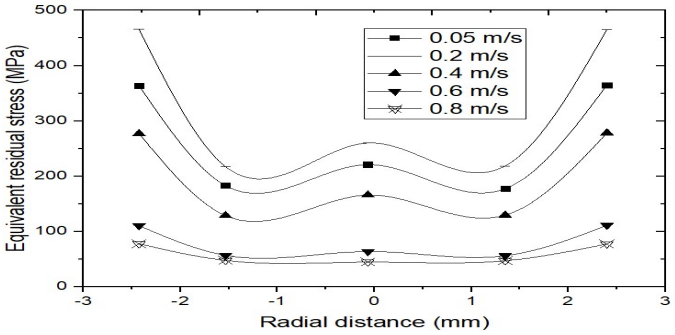

Figure 14: Residual stress variation at different immersion speeds along the radial direction.

Maximum residual stresses of 373.55, 448.04, 278.06 and 77.6 MPa were obtained with immersion speeds of 0.05, 0.2, 0.4, 0.6, and 0.8 m/s., respectively. The increase in immersion speed helps lower residual stress, since there is no enough time for the steel to develop very steep temperature and phase-transformation gradients. As a result, the material cools and transforms more uniformly across its cross-section, which reduces uneven contraction and the buildup of residual stress [23].

Effect of immersion speed on maximum residual stress in the quenched specimen

Fig. 15 shows that immersion speed significantly affects the distribution and magnitude of equivalent residual stress.

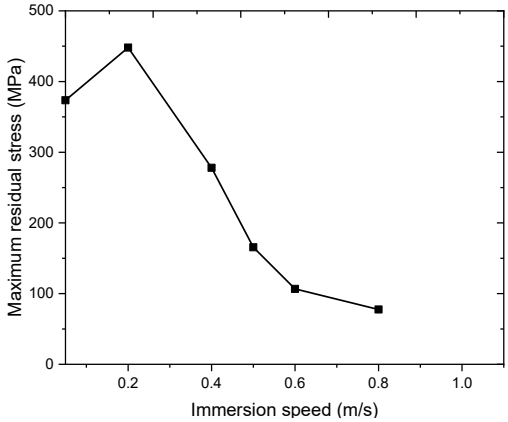

Figure 15: Maximum residual stress in the quenched specimen.

Effect of immersion speed on the microstructure of quenched SAE 1025 steel sample

At equilibrium temperature after quenching, for 0.8 m/s immersion speed, percentage composition of martensite, bainite, ferrite and austenite in quenched SAE 1025 steel was 99.48, 0.19, 0.3,and 0.00249, respectively, as shown in Fig. 16.

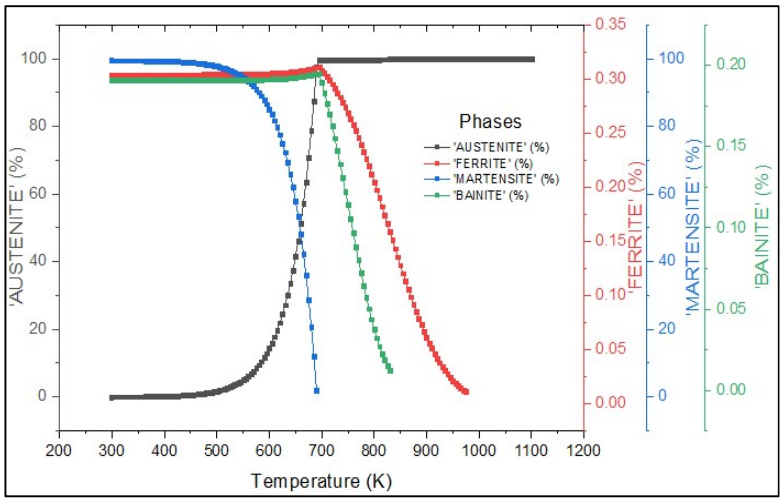

Figure 16: Quench-induced phase distribution at 0.8 m/s.

Effect of quench immersion speed on martensite proportion and strength characteristics of SAE 1025 steel

Fig. 17 shows the effect of immersion speed on martensite composition, tensile strength, yield strength and hardness of quenched SAE 1025 steel, which rises as they increase. Increase in mechanical strength results from greater percentage of martensite composition at a higher immersion speed.

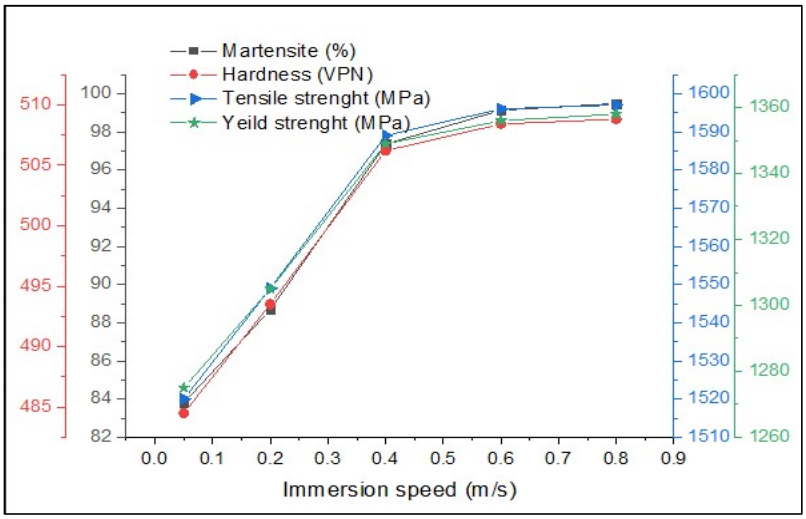

Figure 17: Martensitic response and strength variation with immersion speed.

As the immersion speed increases, martensite composition, tensile strength, yield strength, and hardness of the quenched sample increase. The increase in mechanical strength results from the increase in the percentage of martensite composition at a higher immersion speed. A higher percentage of martensite phase was obtained at higher immersion speed because less time was allowed for diffusion of carbon atoms within the iron lattice, which is necessary for the formation of ferrite and pearlite. Martensite usually forms with a much finer grain structure than microstructures like ferrite or pearlite. These smaller grains create more boundaries, which help resist dislocation movement and enhance the material's strength. This enhances the material strength. Properties that describe mechanical strength (tensile strength, yield strength, and hardness) show identical trends in variation with quench immersion speed. The same metallurgical factors affect their magnitude [30-32].

Effect of diameter on temperature profile and residual stress

Fig. 18 shows temperature profiles generated for specimens with diameters of 5, 7.5 and 10 mm at the geometric center of the specimen, with an immersion speed of 0.4 m/s. It can be observed that a smaller diameter specimen cools faster than a larger one. Cooling times were 2, 3.1 and 13.4 secs, for 5, 7.5 and 10 mm diameter, respectively. This phenomenon occurs because smaller diameter specimens have a higher surface area to volume ratio compared to larger ones. Heat transfer during quenching primarily occurs at the specimen's surface. With a higher surface area relative to its volume, a smaller specimen can dissipate heat more efficiently and rapidly.

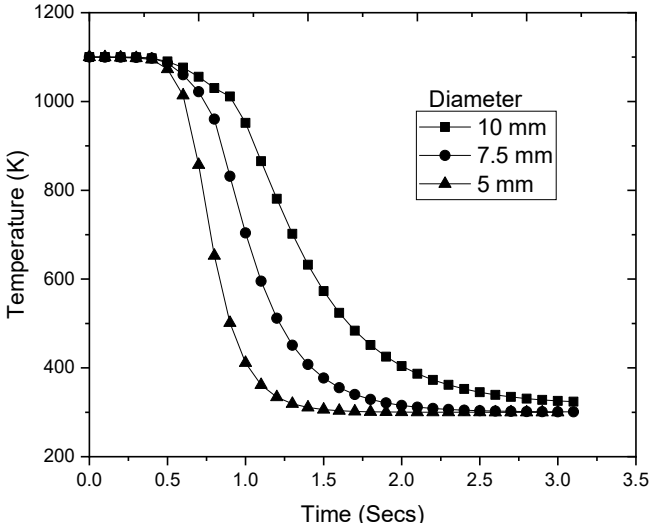

Figure 18: Temperature profile for different specimen diameters.

Fig. 19 shows maximum residual stress generated for different specimen diameters. Maximum residual stresses of 333, 783 and 1042 MPa were obtained for 5, 7.5 and 10 mm diameters, respectively, with 0.4 m/s immersion speed.

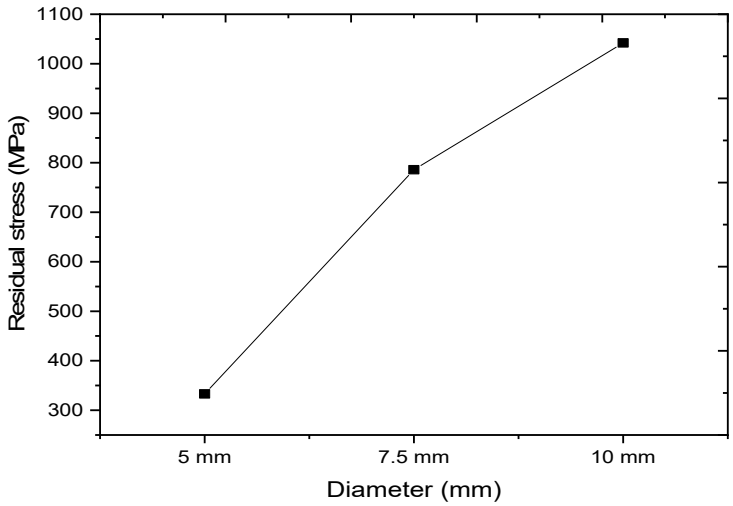

Figure 19: Maximum induced residual stress in samples of different diameters.

It can be observed that maximum residual stress increases with wider diameter of the specimen. In a larger rod, the surface cools and contracts quickly, but the core stays hot much longer, creating a strong thermal gradient. During quenching, the surface forms martensite early, while the core transforms later due to its slower cooling rate. This uneven timing in phase transformation and volume change that comes with martensite formation, creates a transformational gradient. Together, these temperature and transformation differences make larger specimens develop higher internal stresses.

Microstructure of SAE 1025 steel sample after experimental quenching

Increasing immersion speed during quenching has a significant impact on the microstructure of SAE 1025 steel. A higher immersion speed enhances cooling rate, promoting formation of martensite due to suppressed diffusion-controlled transformations. With immersion speeds of 0.2, 0.4, 0.6, and 0.8 m/s, percentages of martensite experimentally obtained from micrograph using ImageJ were 55, 57.5, 65, and 72.95, respectively. This results in a higher rate of martensite and reduced formation of bainite and pearlite. Conversely, slower immersion allows for more bainite and pearlite to form, due to prolonged exposure to intermediate temperatures. Figs. 20 to 23 display micrographs of steel samples quenched at varying immersion speeds, highlighting how changes in cooling rate influence internal grain structure. Microstructural phases were quantified using Fiji (an extended distribution of ImageJ). Micrographs were first converted to grayscale and pre-processed using contrast enhancement and noise-reduction filters. Phase segmentation was then performed by applying an intensity-based threshold, which effectively separated dark martensitic regions from lighter ferritic areas. Segmented phases were labeled, and

their area fractions were directly computed from pixel distribution in the processed image. This approach allowed reliable extraction of martensite and ferrite fractions for comparative analysis [33-39].

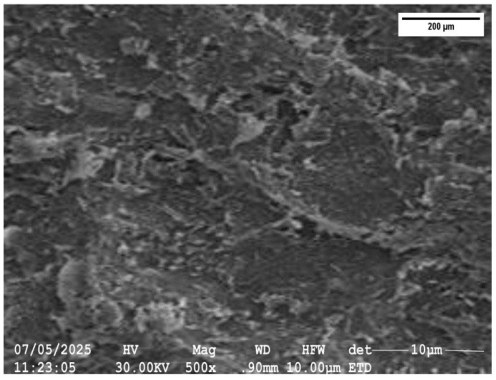

Figure 20: Microstructure of water-quenched steel at an immersion speed of 0.2 m/s (55% martensite and 45% ferrite).

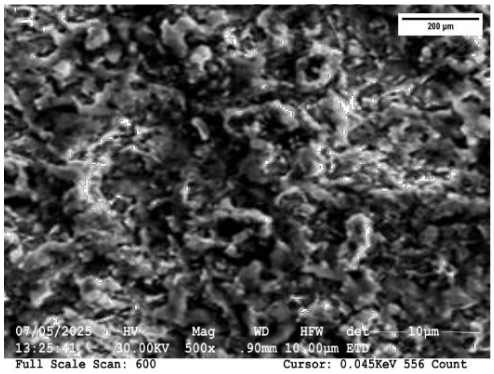

Figure 21: Microstructure of water-quenched steel at an immersion speed of 0.4 m/s (57% martensite and 43% ferrite).

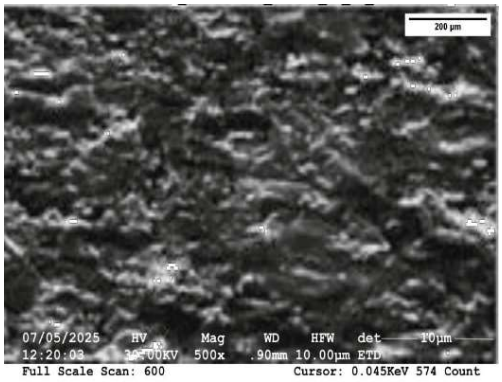

Figure 22: Microstructure of water-quenched steel at an immersion speed of 0.6 m/s (65% martensite and 35% ferrite).

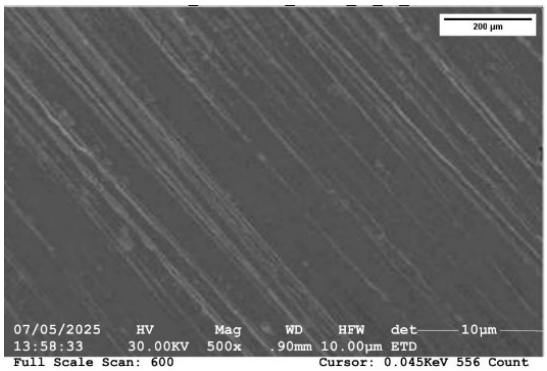

Figure 23: Microstructure of water-quenched steel at an immersion speed of 0.8 m/s (73 % martensite and 27 % ferrite).

Simulated vs. experimental results of hardness, tensile strength, and yield strength after quenching SAE 1025 steel at varying immersion speeds

Comparison between simulated and experimental results for quenching process at varying immersion speeds reveals important insights into mechanical behavior of SAE 1025 steel. There is a general agreement between simulated and experimental data across all measured properties, hardness, ultimate tensile strength and yield strength, though some deviations are evident. For hardness, tensile strength and yield strength (Figs. 24-26), both experimental and simulated values increase with immersion speed, indicating that faster cooling enhances these properties, due to greater martensite formation.

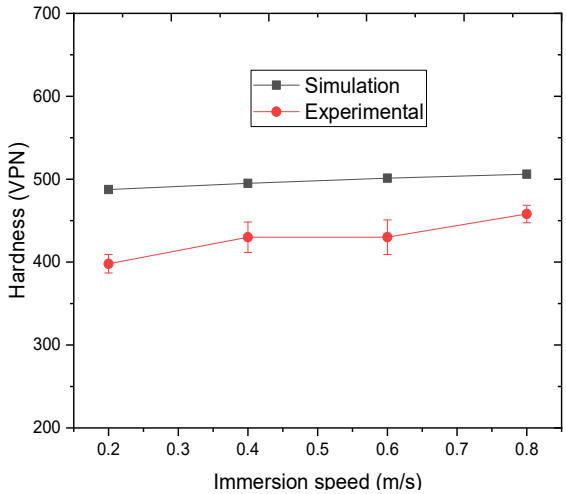

Figure 24: Simulated and experimental hardness at different immersion speed in water.

However, experimental results are slightly lower than simulated ones across all speeds, although the overall pattern is consistent. Aside from possible microstructural irregularities or minor variations in material composition that affect general response

of the material which are not accounted for in the model, one major reason for disparity is time lag in experimental quenching process. This is clearly explained under model validation.

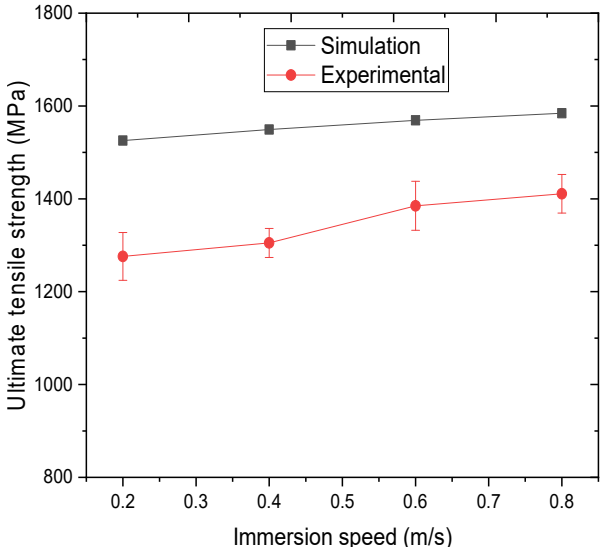

Figure 25: Simulated and experimental tensile strength at different immersion speeds in water.

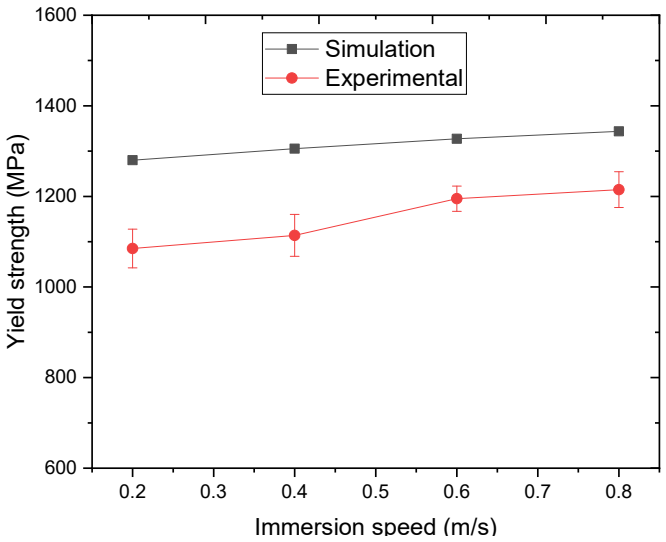

Figure 26: Simulated and experimental yield strength at different immersion speeds in water.

Model validation

To validate the model, its predicted temperature profiles were compared with experimental results recorded at geometric center of a 10 mm diameter specimen quenched at an immersion speed of 0.4 m/s, as shown in Fig. 27.

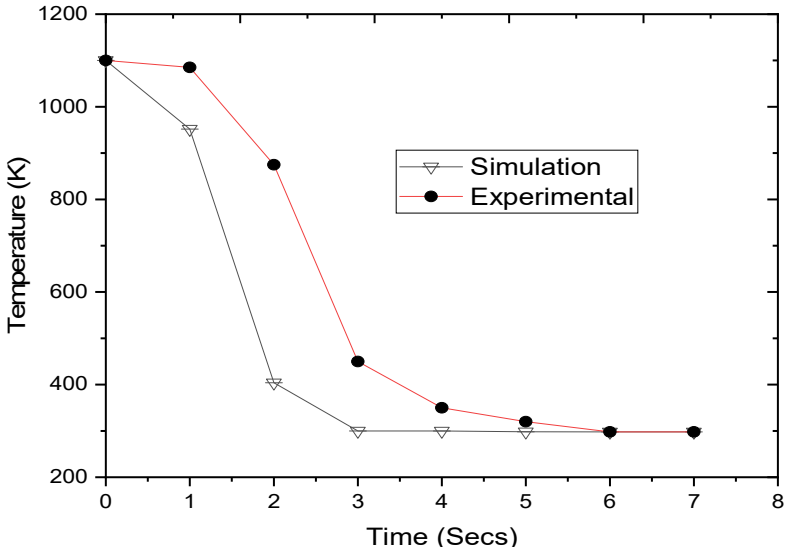

Figure 27: Simulated metal temperature history with experimental data at 0.4 m/s immersion speed in water.

Simulated temperature profile shows a slightly faster cooling rate than experimental data, particularly between 1 and 3 secs. Despite this difference, the two curves converge closely after 4 secs, stabilizing around 300 K. Furthermore, the model's predictive ability was confirmed across a wide range of material properties commonly encountered during direct immersion quenching. In every case, it showed strong agreement with observed results, demonstrating its reliability and accuracy. Average error is 7.5% of total temperature range, and estimated R^2 = is 0.97, indicating a strong correlation between simulated and experimental data.

However, one notable observation in this study is the difference between mechanical strengths obtained from simulation and those measured in practical experiments. Specifically, practical results showed a reduction in strength compared to simulated values. This discrepancy can be explained by the delay that occurred while transferring the heated specimen from the furnace into the quenching bath. Unlike in simulation, where quenching was assumed to take place instantly, ensuring a full martensitic transformation at or above critical cooling rate, in practice, there was a short but noticeable delay during handling. During this period, temperature of the hot specimen fell within bainitic transformation range (864 K) after two secs, being a small-sized specimen due to large area-to-surface ratio. As a result, some bainite formed before the specimen was fully immersed in the quenching medium. This partial transformation led to a mixed microstructure rather than the high percentage martensitic structure predicted in simulation. This difference in cooling history and phase transformation directly affected final mechanical strength of quenched specimen. Bainite generally offers lower hardness and strength compared to

martensite, which explains reduced values observed in practical tests. This highlights the importance of minimizing time between furnace removal and quenching in real-world applications, to achieve properties that closely match simulated expectations.

Comparison of present model with a similar model

Table 2 compares simulated residual stress results from different finite element models with the current work. Equivalent residual stress computed by [28] to predict residual stresses obtained during water quenching of solid cylindrical specimens was employed. Residual stresses at midpoint of a specimen of the same geometry were compared for sequentially coupled analysis. Results were found to be relatively close. The variation could be attributed to differences in properties of quenchant and steel used, as the effect of transformation behavior on residual stress and deformation was not captured in the previous model.

Table 2: Result comparison of residual stress simulation of different models.

Results quantity	Measuring location	Current model	Other model	Relative error in percentage (%)
Equivalent (von Mises) stress	Midpoint	228 MPa	208 MPa	9.6

Conclusion

This study shows clearly that immersion speed, rather than being just another variable, is a powerful and controllable lever for improving quenching performance. As immersion speed increased, cooling rate rose sharply, which helped reduce deformation by 87%, and greatly reduced dimensional instability by limiting steep thermal and transformation gradients.

Residual stress was consistently higher at trailing end and along the specimen surface, mainly because these regions cooled more slowly and developed coarser grains. Even so, raising immersion speed led to 83% drop in maximum residual stress, highlighting how effective faster immersion is at suppressing stress-generating gradients. Larger-diameter samples also trapped more heat and built up higher residual stresses, reinforcing the need for geometry-specific quenching strategies.

Higher immersion speeds encouraged more martensite formation (an 11.24% increase between 0.2 and 0.8 m/s), reduced pearlite/bainite transformation and produced steady improvements in hardness, tensile strength and yield strength.

The numerical model performed well, with temperature predictions aligning closely with experiments (MAE = 7.5%, r = 0.97) and residual stress patterns matching validated models (9.6% difference).

Practically, the study also shows that even a short delay between removing the work piece from the furnace and quenching allows bainitic transformation to begin, which

lowers final strength in a thin component. Keeping transfer time to an absolute minimum is therefore crucial for achieving full benefits of high-speed immersion quenching in real industrial environments

Results clearly indicate that immersion speed, transfer time and part geometry are significant variables. They determine the cooling pathway, phases that form and stresses that occur during quenching. For practical application, the work highlights a few key actions: use higher immersion speeds (around 0.8 m/s or more) when dimensional stability and low residual stress are priorities; keep transfer time below 2-3 s, since even short delays allow bainite to form and reduce strength in smaller parts; adjust immersion speed to suit part geometry, as thick sections hold heat longer and build higher stresses; maintain uniform agitation to avoid delayed cooling at the trailing end and the risk of coarse grains; and integrate numerical modelling into process planning, as predictions closely match real thermal and stress behavior.

In practice, benefits of high-speed immersion quenching only appear when these parameters are tightly controlled. Doing so improves performance, limits distortion and yields more dependable steel components.

Authors' contributions

T.S. Olabamiji: collected data, inserted data; performed analysis, wrote the paper.
S.M. Adedayo: conceived the original idea; supervised the work.

Abbreviations

ASTM: American Society for Testing and Materials
CFD: Computational fluid dynamics
FEM : finite element method
MPa: Mega Pascal
R^2: coefficient of determination
SAE: Society of Automotive Engineers
SEM: scanning electron microscope
VPN: Vickers Pyramid Number
MAE: mean absolute error

Symbols definition

α_k: Phase volume fraction [dimensionless]
ε^{th}: Thermal strain [$1/°C$]
C_p: Specific heat capacity [$J\ kg^{-1}$]
E_k: phase enthalpy [($J\ kg^{-1}\ K^{-1}$]
F: Body force [N]
h_f: Fluid local heat transfer coefficient [W/m^2K]
h_k: Phase sensible enthalpy [kJ]s

k_{eff}: effective conductivity
K_t: turbulence thermal conductivity [W/[m·K]]
ρ_k: phase density [kg/m^3]
ρ_m: mixture density [kg/m^3]
P: pressure [N/m^2]
Q: heat generation rate per unit volume [W/m^3].
q_{rd}: radiative heat transfer [$J/s\ m^2\ K^4$]
S_E: volumetric heat source [$J/(m^3 \cdot K)$]
t: time [s]
T: temperature [K]
T_f: local fluid temperature [K]
T_w: wall surface Temperature [K]
μ_m: viscosity of the mixture [N s m^{-2}]
v: mass average velocity [m/s]
$\mathbf{v}_m$: mixture velocity [m/s]
$\mathbf{v}_{dr,k}$: phase drift velocity [m/s]

References

1. Ghasri-Khouzani M, McDermid JR. Effect of carbon content on the mechanical properties and microstructural evolution of Fe-22Mn-C steels. Mater Sci Eng A. 2015;621:118-27. https://doi.org/10.1016/j.msea.2014.10.042
2. De la Concepción VL, Lorusso HN, Svoboda HG. Effect of Carbon Content on Microstructure and Mechanical Properties of Dual-Phase Steels. Proced Mater Sci. 2015;8:1047-56. https://doi.org/10.1016/j.mspro.2015.04.167
3. Kumar K, Arya HK. Experimental Determination of Cooling Rate and Its Effect on Microhardness in Submerged Arc Welding of Mild Steel Plate (Grade C-25 as per IS 1570). J Mater Sci Eng. 2013;03(02):3-6. https://doi.org/10.4172/21690022.1000138
4. Nagie JM. The Effect of Cooling Rate on Mechanical Properties of Carbon Steel (St 35). Diyal J Eng Sci. 2014;07(01):109-18. https://doi.org/10.24237/djes.2014.07108
5. Pyshmintsev IY, Boryakova AN, Smirnov MA. Effect of cooling rate on the structure and properties of low-carbon tube steel. Metallurgist. 2008;52(7):48-51. https://doi.org/10.1007/s11015-008-9081-4
6. Bucquet T, Sander S, Fritsching U. Characterization of Spray Nozzles for Quenching of Metal Components. ILASS Eur. 26th Annu Conf Liq at Spray Syst. 2015. https://doi.org/10.13140/2.1.3629.0881
7. Funatani K. Distortion control via optimization of the cooling process and improvement of quench oils. J Mech Eng. 2009;55(3):182-90.

8. Xia P, Sabirov I, Molina-Aldareguia J et al. Mechanical behavior and microstructure evolution of a quenched and partitioned steel during drop weight impact and punch testing. Mater Sci Eng. 2018;737:18-26. https:doi.org/10.1016/j.msea.2018.09.015
9. Jodia W, Alfatlawi SHA, Jasim HH et al. Review on Heat Treatments of Carbon Steel. Iraqi J Mech Mater Eng. 2024;23(2):42-58. https:doi.org/10.32852/4kykqp25
10. Deng Y, Li Z, Chen J et al. The effects of the structure characteristics on magnetic Barkhausen noise in commercial steels. J Magn Magn Mater. 2018;451:276-82. https:doi.org/10.1016/j.jmmm.2017.11.041
11. Joseph OO, Joseph OO, Leramo RO et al. Effect of Heat Treatment on Microstructure and Mechanical Properties of SAE 1025 Steel: Analysis by one-way ANOVA. J Mater Environ Sci. 2015;6(1):101-06.
12. Adedayo SM, Adekunle AS, Oladimeji T. Effect of Quench Immersion Speed in Water on the Mechanical Properties of C30 Carbon Steel. Proceedings of the WCE. 2014; Vol II. London, U.K.
13. Agboola JB, Abubakre OK, Mudiare E et al. Effects of Bath Temperature on Cooling Rate, Mechanical Properties, and Microstructure of Medium Carbon Steel during Quenching Operations. J E Technol Pol. 2015;5(3):18-26.
14. Alam U. Experimental Study of Local Heat Transfer during Quenching of Metals by Spray and Multiple Jets. 2011. Dissertation.
15. Penha RN, Chiqueti CM. Influence of Agitation Rate on Residual Stresses and Distortion on Quenched AISI 5160 Steel. SAE Technical Paper Series, 2018.
16. Pola A, Gelfi M, La Vecchia GM. Simulation and validation of spray quenching applied to heavy forgings. J Mater Process Technol. 2013;213(12):2247-53. https://doi.org/10.1016/j.jmatprotec.2013.06.019
17. Xun ZY, Ping YY, Quan HS et al. Influence of quenching cooling rate on residual stress and tensile properties of 2A14 aluminum alloy forgings. Mater Sci Eng A. 2016;674:658-65. https://doi.org/10.1016/j.msea.2016.08.017
18. López-García RD, García-Pastor FA, Maldonado-Reyes A et al. Analysis of the effect of immersion rate on the distortion and residual stresses in quenched SAE 5160 steel using FEM. J Mater Res Technol. 2019;8(6):5557-71. https://doi.org/10.1016/j.jmrt.2019.09.024
19. Kuznetsov AA, Rudnev VI. Causes of Cracking in Quenching of the Parts Made of Steels and Cast Iron and Recommendations for Their Removal: A Review 1. Russ Metall (Met). 2017;13:1125-30. https://doi.org/10.1134/S0036029517130158
20. Sedighi M, McMahon CA. The influence of quenchant agitation on the heat transfer coefficient and residual stress development in the quenching of steels. Proc Inst Mech Eng Part B J Eng Manuf. 2015;214(7):555-67. https://doi.org/10.1243/0954405001518251

21. Krause F, Schüttenberg S, Fritsching U. Modelling and simulation of flow boiling heat transfer. Int J Numer Meth Heat Fluid Flow. 2010;20(3):312-31. https://doi.org/10.1108/09615531011024066
22. Gallitelli D, Vincent B, Maxime G et al. Simulation of shot peening : From process parameters to residual stress fields in a structure. Comp Rend Mec. 2016;344(4-5):355-74. https://doi.org/10.1016/j.crme.2016.02.006
23. Lopez-Garcia RD, Medina-Juárez I, Maldonado-Reyes A. Effect of Quenching Parameters on Distortion Phenomena in AISI 4340 Steel. Metals. 2022;12(5). https://doi.org/10.3390/met12050759
24. Sarker P. Investigation of the Quenching Characteristics of Steel Components by Static and Dynamic Analyses. Proceedings of the ASME. Mech Eng Cong Exp. 2014. https://doi.org/10.1115/IMECE2014-3870. Thesis
25. Passarella DN, Varas F, Martín EB. Heat transfer model for quenching by submerging. J Phys Conf Ser. 2011;296(1):012004. https//doi.org/10.1088/1742-6596/296/1/012004
26. Lei C, Arkaprabha S, Daniel P et al. Effect of texture and grain size on the residual stress of nanocrystalline thin films. Mod Simul Mater Sci Eng. 2017;25(7):7500. https://doi.org/10.1088/1361-651X/aa80fb
27. Xiao LC. Computer simulation of the thermal-mechanics of steel quenching. Oregon Grad Inst Sci Technol. 1998. Thesis
28. Sen S, Aksakal B, Ozel A. Transient and residual thermal stresses in quenched cylindrical bodies. Int J Mech Sci. 2000;42(10):2013-29. https://doi.org/10.1016/S0020-7403(99)00063-6
29. Pratik S, Uttam C. Analysis of the Residual Stress and Deformation in a Steel Tube due to Quenching Process using Different Media. Proceed ASME Int Mech Eng Congr Expo. 2014:1-10. https://doi.org/10.1115/IMECE2014-38701
30. Bagliani EP, Santofimia MJ, Zhao L et al. Microstructure, tensile, and toughness properties after quenching and partitioning treatments of a medium-carbon steel. Mater Sci Eng A. 2013;559:486-95. https://doi.org/10.1016/j.msea.2012.08.130
31. Limbasiya N, Jain A, Soni H et al. A comprehensive review on the effect of process parameters and post-process treatments on microstructure and mechanical properties of selective laser melting of AlSi10Mg. J Mater Res Technol. 2022;21:1141-76. https//doi.org/10.1016/j.jmrt.2022.09.092
32. Olumide T, Lu J. Literature review on the mechanical properties of materials after surface mechanical attrition treatment (SMAT). Nano Mater Sci. 2020;2(1):3-31. https// doi.org/10.1016/j.nanoms.2020.04.002
33. Sinha V, Gonzales M, Payton EJ. Microstructural Refinement in a Low-Alloy High-Strength Martensitic Steel. Metall Microstruct Analy. 2025;14(2):404-21. https:/doi.org/10.1007/s13632-024-01162-2

34. Toraman S, Cosgun T, Alkan B et al. Assessing the volume fractions of the phases, nodularity, and nodule count of spheroidal graphite cast iron using ImageJ software. Mugl J Sci Tech. 2019;5(1):137-42. https://doi.org/10.22531/muglajsci.521128
35. Ireti AF, Omeiza AE, Oluwasegun EK et al. Comparison of ImageJ Analysis of the Structure of Two Constructional Steels. Am J Eng Appl Sci. 2018;1(1):318-26. https://doi.org/10.3844/ajeassp.2018.318.326
36. Strakošová A, Daniel K, Flip P et al. Microstructural and mechanical insights into 1.2709 maraging steel produced by direct energy deposition. J Mater Sci. 2025;60:17933-52. https://doi.org/10.1007/s10853-025-11439-8
37. Tajmiri S, Haider W, Shabib I. Effect of Heating Rate on Microstructure and Corrosion Resistance Quenched and Tempered 8620 Low Carbon Alloy Steel. Corros Mater Degrad. 2024;5:370-86. https://doi.org/10.3390/cmd5030016
38. Sikora E, Ferenc K, Dora T. Microstructure and phase evolution in increasing the amount of mo and Ti of non-equiatomic CoFeNi-based medium entropy alloys for organic wastewater treatment. Sci Rep. 2025;15(1):18835. https://doi.org/10.1038/s41598-025-03976-8
39. Azevedo A, Nicolodi A, Deves B et al. Automated procedure for coke microstructural characterization in imagej software aiming industrial application. Fuel. 2021;304: 121374. https://doi.org/10.1016/j.fuel.2021.121374